Wideband Transmitarray With Reduced Profile

Qi Luo, *Member, IEEE*, Steven Gao, *Senior Member, IEEE*, Mohammed Sobhy, *Life Member, IEEE*, and Xuexia Yang, *Member, IEEE*

***Abstract*—This letter presents a wideband transmitarray (TA) with reduced profile. A novel unit cell based on a wideband bandpass filter is developed and applied to the design of the TA. The TA consists of two identical trilayer frequency selective surfaces (FSSs), thus it has a lower profile compared to traditional designs that use at least four FSS layers separated by quarter-wavelength air gaps to obtain the 360° phase shift range. The FSS has a pair of square patches printed on the top and bottom layers, and a square slot loaded by four microstrip lines printed on the middle layer. The phase shift is achieved by simultaneously adjusting the size of the square patches. Within the frequency band of interest, the developed unit cell shows low insertion loss and sufficient phase shift range. An equivalent circuit model is developed to better understand the operating principles of the FSS. To validate the design concept, one prototype operating at 13.5 GHz is designed, fabricated, and measured. The measurement results show that the designed TA achieves 16% 1 dB gain bandwidth and 60% aperture efficiency. The developed unit cell has symmetric configurations so it can also be applied to the design of dual-polarized or circularly polarized TAs.**

***Index Terms*—Frequency selective surface, low profile, transmitarray (TA), wideband.**

I. Introduction

HIGH-GAIN, wideband, and lightweight antennas are highly desirable for many wireless systems, such as satellite communications [1]. Compared to the phased array antennas, reflectarrays and transmitarrays (TAs) avoid the use of feed networks, thanks to the space-fed technique, while providing comparable radiation performances at their operation frequencies [2]. Thus, they have received much research interest recently.

A TA consists of one or multiple feed antennas and an array of unit cells. Compared to reflectarrays, TAs place the feed antenna in front of the aperture without incurring any blockage losses. This is especially advantageous when there is a need for using multiple feeds to obtain multibeams or beam-switching [3], [4]. Generally speaking, there are two approaches to design TAs. The first approach is based on the array antenna, where one array antenna receives the RF signal from the feeding source and transmits to another array antenna, which retransmits the RF signal with preadjusted phase to form a co-phasal beam in the far field [5]–[7]. Due to the narrow bandwidth of the radiating element and the insertion loss resulting from the "receive–transmit" configuration, using this approach the TA normally has a narrow bandwidth. For example, in [7], the TA unit cell consists of two identical square patch antennas that were separated by a copper ground plane, and the two patches were connected by a via. The reported 1 dB transmission bandwidth of the unit cell is only 6.5%. Another approach is based on frequency selective surfaces (FSSs). This approach uses FSS as "free-space phase shifter" to obtain the desired phase delays to form the focused beam. Because of the low insertion loss and wide bandwidth of the FSS, the resulting TA has a wide bandwidth and high efficiency. However, to achieve a phase shift range of 360°, normally multiple layers of FSSs separated by a distance of quarter-wavelength is needed [8], which leads to a relatively high profile. In [8], a wideband TA with 11.7% 1 dB gain bandwidth was presented. This reported TA has four conductive layers, and each layer is printed on a separated substrate. Between each substrate, there is an approximately quarter-wavelength air gap, and the total thickness of this TA is 0.76λ. Another wideband TA using similar configuration was reported in [9], which also uses four conductive layers printed on four substrates spaced by air gaps to obtain the 360° phase shift range. The reported 1 dB gain bandwidth is 15% with a total thickness of 0.65λ.

There are several reported works on reducing the profile of the FSS-based TA designs while maintaining the 360° phase shift range of the unit cell. For example, a TA element with two layers of modified Malta crosses was presented in [10]. To increase the phase shift range, four vias are employed on each unit cell. Although the profile of the antenna was reduced, the 1 dB gain bandwidth decreased to 5.9%. A low-profile TA based on spatial phase shifters was reported in [11]. The unit cell consists of three capacitive and two inductive layers. Although this TA unit cell has a thin thickness, it has a relatively narrow bandwidth and low efficiency. Moreover, the sizes of the capacitive patches at each layer are different, which increases the synthesize complexity when higher order FSS is used.

In this letter, a novel TA unit cell based on a wideband bandpass FSS is presented. The developed FSS has three layers printed on two substrates. The TA unit cell consists of two such FSSs separated by a quarter-wavelength air gap, and by using this unit cell, a wideband TA with a reduced profile and high efficiency operating at 13.5 GHz was designed, fabricated, and measured. Compared to other reported TA designs of

Manuscript received October 29, 2017; revised January 4, 2018; accepted January 14, 2018. Date of publication January 17, 2018; date of current version March 1, 2018. This work was supported by the EPSRC Project under Grant EP/N032470/1. *(Corresponding author: Qi Luo.)*

Q. Luo, S. Gao, and M. Sobhy are with the Department of Engineering and Digital Arts, University of Kent, Canterbury CT2 7NZ, U.K. (e-mail: qiluo@ieee.org; s.gao@kent.ac.uk; M.I.Sobhy@kent.ac.uk).

X. Yang is with the School of Communication and Information Engineering, Shanghai University, Shanghai 200444, China (e-mail: xxyang@staff.shu.edu.cn).

Digital Object Identifier 10.1109/LAWP.2018.2794605

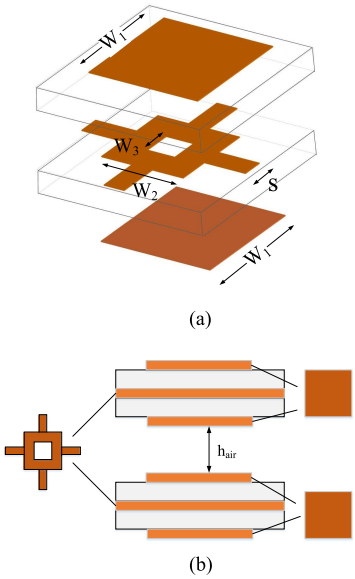

Fig. 1. (a) Exploded and (b) side view of the unit cell of the TA. The copper is represented by the color bronze.

similar gain bandwidth [8], [9], the presented design reduces the profile to 0.36λ while maintaining the wideband operation with promising aperture efficiency. Because the trilayer FSS is printed on two substrates and does not require any vias, the present design can be fabricated using standard printed circuit board (PCB) process with relatively low fabrication cost. This letter is organized as follows. Section II details the design and analysis of the TA unit cell. Section III presents the design of the TA, as well as the simulation and measurement results of the prototype. Section IV concludes the letter.

II. Design of the TA Unit Cell

Fig. 1 shows the configuration of the developed unit cell. The unit cell consists of a pair of trilayer frequency selective surfaces separated by a distance of quarter-wavelength at the frequency of interest. As shown in Fig. 1, the two square patches and one square loop with four microstrips are printed on two dielectric substrates of the same type. The unit cell has a symmetrical configuration that makes it also suitable for dual-polarization or circularly polarized applications.

The trilayer FSS is a wideband bandpass filter, and the wideband response of the FSS is achieved by creating a second-order passband response. To achieve such response, a combination of capacitive and inductive layers printed on two substrates is required [12]. To better understand the operation mechanism of the FSS, the equivalent circuit model of the trilayer FSS is developed and is shown in Fig. 2. To simplify the analysis, this model assumes that there is no loss from the dielectric and the conductor. The square patch, which is printed on the first and third layers, is modeled as a parallel *LC* circuit (L_1 and C_1). Layer two can be regarded as a combination of a square loop in parallel with inductive microstrips. The square loop is modeled as a parallel *LC* circuit (L_4 and C_4) in series with two inductors (L_3), and the conductive strips are modeled as a series *LC* circuit (L_2 and C_2). The capacitance C_5 is the coupling between

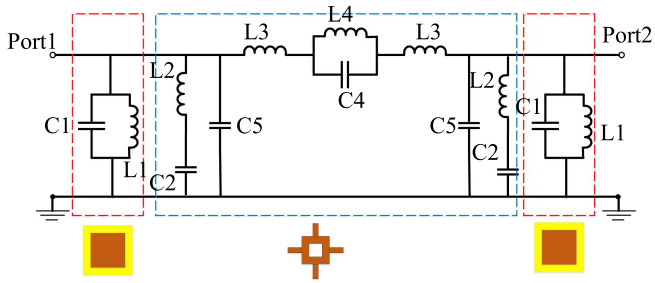

Fig. 2. Equivalent circuit model of the trilayer FSS working as a wideband passband filter.

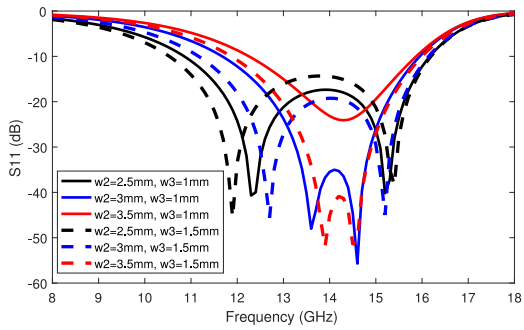

Fig. 3. Simulated reflection coefficient of the FSS with varied size of W_2 and W_3.

different layers. By adjusting the size of the square loop (W_2 and W_3) in the second layer, the two passbands can be tuned to achieve a wideband response. In the equivalent circuit model, changing the size of the square loop is equivalent to adjusting the values of L_4, C_4, and L_3. Fig. 3 shows the simulated reflection coefficient of the FSS with varied size of W_2 and W_3. In these simulations, the unit cell is chosen to operate at 13.5 GHz. The unit cell has a period of 6 mm and is printed on two Roger 4003C substrates ($\varepsilon_r = 3.55, \tan\sigma = 0.0027$) with thickness of 0.8 mm. The simulations were performed by using periodic boundary conditions with Floquet ports in the electromagnetic (EM) simulator Ansys HFSS. As shown, the second layer contributes to multiple resonances of the FSS, and it controls the frequency ratio between these two resonances. These values are optimized in order to obtain the minimum insertion loss at the frequency band of interest. The values of the final optimized parameters are: $W_1 = 4$ mm, $W_2 = 3$ mm, $W_3 = 1$ mm, $s = 0.75$ mm, $h_{\text{air}} = 4.9$ mm, $P = 6$ mm, $L_s = 1.5$ mm, and $t_{\text{diel}} = 0.8$ mm. Fig. 4 compares the simulated transmission and reflection coefficients of the trilayer FSS using the EM simulator and the equivalent circuit model. As can be seen, there is a good agreement between EM simulation and the circuit simulation results. Values of the circuit components were first calculated by using microstrip theories, then extracted by performing curve fitting using the EM simulation results.

The phase shift of the unit cell is achieved by simultaneously varying the width (W_1) of the patches printed on the first and third layers. Thus, the synthesis of the unit cell is very simple because it only has one variable. Fig. 5 shows the phase and amplitude of the transmission coefficient of the unit cell shown in Fig. 1 when W_1 varies. As shown, when the W_1 changes from 1.8 to 4.8 mm, a 360° phase shift is obtained. Within most of

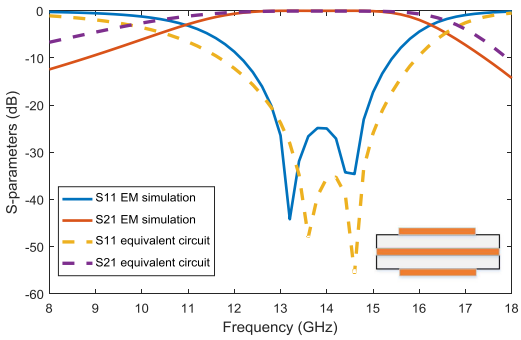

Fig. 4. Transmission and reflection coefficients of the trilayer FSS using the EM simulation and the equivalent circuit model.

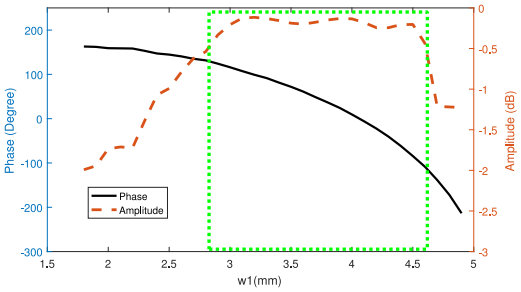

Fig. 5. Phase and amplitude of the transmission coefficient of the unit cell with varied values of W_1 at 13.5 GHz.

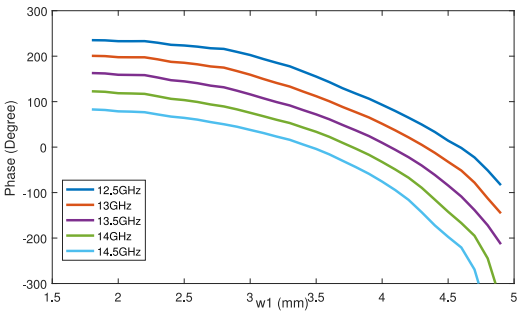

Fig. 6. Simulated phase shift of the unit cell at different frequencies with varied values of W_1.

this region, as indicated by the green dashed box, the insertion loss is less than 0.5 dB. As will be presented later, this region is used to design the central elements of the TA. Fig. 6 shows the phase shift of the unit cell at different frequencies when W_1 varies. As can be seen, within the 2 GHz frequency range, the phase shift curves are parallel, which implies that the unit cell provides a wideband response.

Fig. 7 shows the simulated transmission coefficient of the unit cell with different incident angles. The unit cell has a very stable response except for some slight shifting on the lower cutoff frequencies when the incident angle increases to 40°. Despite that, the passband always covers the frequency band of interests with low insertion loss.

III. Design of the TA and Experimental Results

To validate the developed wideband TA unit cell, a prototype TA antenna that operates at 13.5 GHz band with broadside

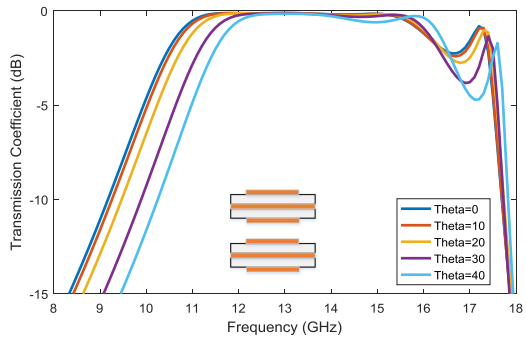

Fig. 7. Simulated transmission coefficient of the unit cell with different incident angles.

radiation is designed, fabricated, and measured. The dimension of the TA is 90 mm × 90 mm × 8.1 mm, corresponding to a thickness of $0.36\lambda_{13.5\text{ GHz}}$. There are 225 unit cells positioned in a square aperture. A linearly polarized corrugated circular horn antenna is used as the feed antenna and is placed at a distance of 90 mm above the center of the planar array, corresponding to a focal/diameter (f/D) ratio of 1. The gain of the feed horn is about 15 dBi. The value of f/D was chosen to one considering the illumination tapering at the edge of the TA surface is about 9 dB. The cross-polar discrimination (XPD) of the circular horn antenna is around 25 dB.

The size of the square patch W_1 is varied to obtain the desired phase delays while the rest of the parameters remain unchanged. As shown in Fig. 5, when W_1 varies from 2.8 to 4.6 mm, within a phase shifting range of 250°, the insertion loss is less than 0.5 dB. Thus, to reduce the insertion loss and improve the radiation efficiency of the TA, it is necessary to position these unit cells in the center of the planar array where most of the incident energy from the feed is concentrated. This is achieved by introducing an additional reference phase (Δph) when calculating the required phase for each radiating element

$$\Delta\text{ph} = \phi^{'} + \phi_{\text{Max}} - \phi_{\text{Min}} \tag{1}$$

where ϕ_{Max} and ϕ_{Min} are maximum and minimum values of the calculated ϕ_R within the aperture of the TA, respectively. $\phi^{'}$ is phase delay of the unit cell that has low insertion loss. Fig. 8 shows a photograph of the fabricated prototype mounted in the anechoic chamber. The circular horn antenna is fixed to a circular plate where four 12 mm diameter Nylon rods are attached to support the PCBs. During the measurement, the metal plate is covered by microwave absorbers.

Fig. 9 shows the measured and simulated radiation patterns of the TA in the E-and H-planes at 13.5 GHz. In general, there is good agreement between the measurement and simulation results. The measurement results show that the sidelobes are at least 15 dB lower than the main beam. Compared to the simulation results, the measured sidelobes are higher. There are two reasons that cause this disagreement. The first reason is the possible phase errors of the TA elements, which are from the PCB fabrication and multilayer assembling inaccuracy. Another reason is that the feed antenna has higher spillover than the simulation, which is caused by the inaccuracy of the simulation

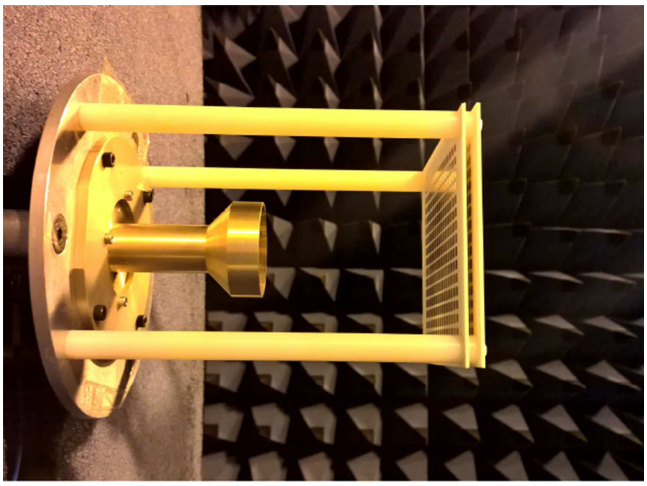

Fig. 8. Fabricated prototype under measurement in the anechoic chamber.

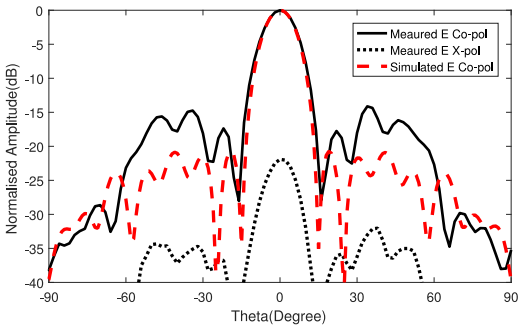

(a)

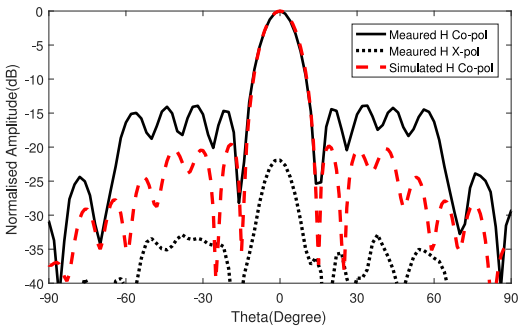

(b)

Fig. 9. Simulated and measured radiations patterns of the prototype at 13.5 GHz in (a) E-plane and (b) H-plane.

model of the corrugated horn antenna and alignment tolerances of the feed antenna. The measured XPD is higher than 20 dB within the entire frequency band of interest. Considering that the XPD of the feed antenna is around 25 dB, the cross polarization of the TA is quite low. The simulated cross polarizations are not shown in these figures because during the simulation one ideal horn was used and the simulated XPD was higher than 55 dB. Fig. 10 shows the measured and simulated gain variation of the designed TA within its operating frequency band. The measurement shows that from 12 to 14.5 GHz, the gain variation is within 1.5 dB, representing a fractional bandwidth of 18.5%. The 1 dB gain variation bandwidth is 16%.

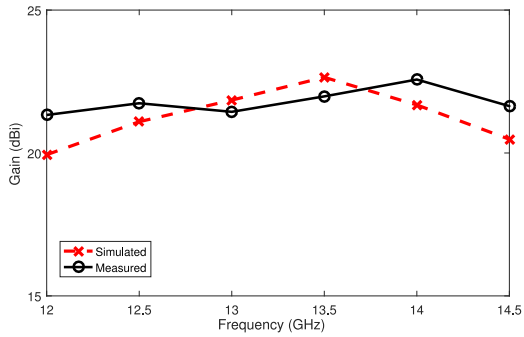

Fig. 10. Gain variation of the present TA.

IV. Conclusion

In this letter, a wideband TA with the reduced profile is presented. By stacking two of the developed novel trilayer FSS as the unit cell, the designed TA reduces its profile compared to traditional designs while maintaining wide bandwidth and promising efficiency. Good agreement between the simulation and measurement results are obtained, showing that the TA has 16% 1 dB gain bandwidth with the maximum aperture efficiency of 60%. The present design concept is scalable, and it can be scaled to design TAs at different operation frequencies. Moreover, the developed unit cell has a symmetrical configuration so it can also be applied to the design of dual-polarized TAs.

References

[1] W. Imbriale, S. Gao, and L. Boccia, Eds., *Space Antenna Handbook*. New York, NY, USA: Wiley, 2012.

[2] Q. Luo *et al.*, "Design and analysis of a reflectarray using slot antenna elements for ka-band satcom," *IEEE Trans. Antennas Propag.*, vol. 63, no. 4, pp. 1365–1374, Apr. 2015.

[3] Y. S. Zhang and W. Hong, "A millimeter-wave gain enhanced multi-beam antenna based on a coplanar cylindrical dielectric lens," *IEEE Trans. Antennas Propag.*, vol. 60, no. 7, pp. 3485–3488, Jul. 2012.

[4] A. Moknache *et al.*, "A switched-beam linearly-polarized transmitarray antenna for V-band backhaul applications," in *Proc. 10th Eur. Conf. Antennas Propag.*, Apr. 2016, pp. 1–5.

[5] A. Clemente, L. Dussopt, R. Sauleau, P. Potier, and P. Pouliguen, "1-bit reconfigurable unit cell based on pin diodes for transmit-array applications in x -band," *IEEE Trans. Antennas Propag.*, vol. 60, no. 5, pp. 2260–2269, May 2012.

[6] J. Y. Lau and S. V. Hum, "A wideband reconfigurable transmitarray element," *IEEE Trans. Antennas Propag.*, vol. 60, no. 3, pp. 1303–1311, Mar. 2012.

[7] H. Kaouach, L. Dussopt, J. Lanteri, T. Koleck, and R. Sauleau, "Wideband low-loss linear and circular polarization transmit-arrays in v-band," *IEEE Trans. Antennas Propag.*, vol. 59, no. 7, pp. 2513–2523, Jul. 2011.

[8] A. H. Abdelrahman *et al.*, "Bandwidth improvement methods of transmitarray antennas," *IEEE Trans. Antennas Propag.*, vol. 63, no. 7, pp. 2946–2954, Jul. 2015.

[9] H. Nematollahi, J. J. Laurin, J. E. Page, and J. A. Encinar, "Design of broadband transmitarray unit cells with comparative study of different numbers of layers," *IEEE Trans. Antennas Propag.*, vol. 63, no. 4, pp. 1473–1481, Apr. 2015.

[10] W. An, S. Xu, F. Yang, and M. Li, "A double-layer transmitarray antenna using Malta crosses with vias," *IEEE Trans. Antennas Propag.*, vol. 64, no. 3, pp. 1120–1125, Mar. 2016.

[11] M. A. Al-Joumayly and N. Behdad, "Wideband planar microwave lenses using sub-wavelength spatial phase shifters," *IEEE Trans. Antennas Propag.*, vol. 59, no. 12, pp. 4542–4552, Dec. 2011.

[12] M. Al-Joumayly and N. Behdad, "A generalized method for synthesizing low-profile, band-pass frequency selective surfaces with non-resonant constituting elements," *IEEE Trans. Antennas Propag.*, vol. 58, no. 12, pp. 4033–4041, Dec. 2010.